ELSEVIER

Ceramics International 29 (2003) 305–309

CERAMICS INTERNATIONAL

www.elsevier.com/locate/ceramint

The microstructural features of an alumina–mullite–zirconia refractory material corroded by molten glass

Cemail Aksel*

Department of Materials Science and Engineering, Anadolu University, Iki Eylül Campus, 26555 Eskisehir, Turkey

Received 17 June 2002; accepted 20 July 2002

Abstract

An alumina-mullite-zirconia refractory penetrated by a standard soda-lime-silica glass was statically tested at 1370 °C for 72 h. Microstructural features and EDAX analysis of the compositions in the corroded region were examined by SEM. During penetration, alumina particles started dissolving in the glassy-phase; and thus randomly oriented needle-like alumina crystals were formed and began growing up in the penetrated region. On the other hand, zirconia made an effective barrier in the corroded zone, and therefore the formation of needle-like alumina crystals disappeared steadily towards to the end of the penetration region, with a low solubility rate of SiO_2, Na_2O and CaO, leading to a high corrosion resistance of the refractory.

Keywords: C. Corrosion; D. Glass; D. Mullite; D. Al_2O_3; D. ZrO_2; E. Refractories; Zircon

1. Introduction

The addition of either zircon ($ZrSiO_4$) or ZrO_2 into alumina–mullite refractories promotes the densification of refractories: when $ZrSiO_4$ dissociates into ZrO_2 and SiO_2, the formation of a glassy phase (SiO_2) may improve the densification through liquid phase sintering [1]. Zircon does not undergo any structural transformation until its dissociation temperature of ~1675 °C [2]; however, the existence of some impurities in the starting powder may reduce the decomposition temperature [3]. Mechanical and thermal shock properties of refractories can be enhanced by the addition of either $ZrSiO_4$ or ZrO_2 [4]. The improvement in mechanical properties was attributed to the tetragonal to monoclinic phase transformation of particles in a zone at the tip of a propagating crack [5–7].

AMZ refractories used in the glass industry are subject to thermal shock stresses during installation. Once installed, the service life of the refractory is then determined for the most part by its corrosion characteristics [8]. Slip cast AMZ compositions can be achieved by batching cheaper zirconium silicate rather than expensive pure zirconia. It has been reported that higher levels of zirconia are known to increase manufacturing difficulties [9]. Refractories with high zirconia contents (>50 wt.%) do not offer improved corrosion resistance to glass. There is an optimum mixture of alumina and zirconia that has corrosion resistance superior to either alumina or zirconia in glass [9].

Slip cast alumina–mullite–zirconia (AMZ) refractories are widely used in the forehearth, distributor, feeders, and glass melting furnaces, as glass refractories, such as plungers, spouts, tubes, stirrers, channels, rotor segments, mantle blocks, orifice rings [8,10]. The widespread usage of this class of materials due to the their high corrosion resistance can be attributed primarily to the unique microstructural features, including the interlocking of alumina crystals and the glassy matrix with the almost insoluble ZrO_2 crystals [9,11].

When a refractory material containing zirconia is being penetrated by glass, glassy phases in the corroded area are found to exhibit randomly oriented needle-like crystals [11]. The previous workers [12] have suggested that these grains are mullite; however, scanning electron microscopy (SEM) and transmission electron microscopy (TEM) indicates that at least some of them are corundum in the interface region penetrated by glass, where alumina is entirely dissolved in the glass phase.

* Tel.: +90-222-335-0580 ext. 6355; fax: +90-222-323-9501.
E-mail address: caksel@anadolu.edu.tr (C. Aksel).

0272-8842/03/$22.00
PII: S0272-8842(02)00137-2

Table 1
EDAX analysis of the compositions of each numbered zone (indicated in Fig. 1), from glass (g) to the refractory (r) side, with a distance of ~500 μm length

Compounds	Chemical analysis of glass (g), refractory (r) and each numbered zone in the interface region (%)						
	g	1	2	3	4	5	r
Na_2O	8.7	6.6	5.3	4.5	4.8	4.0	0.4
Al_2O_3	24.4	43.2	49.7	53.2	50.9	52.2	67.6
SiO_2	59.2	30.2	26.4	24.1	27.2	24.2	18.6
K_2O	0.5	0.2	0.3	0.3	0.4	0.2	0.2
CaO	7.2	5.7	2.7	1.5	0.9	0.6	0.1
ZrO_2	–	14.0	15.6	16.4	16.0	18.7	13.1

Zirconia is found to be more durable phase than alumina and thereby improves the overall corrosion resistance of the refractory body. The rate of corrosion is controlled by the transportation of zirconia into bulk glasses, in which the effect of CaO in glasses is significant, as well as that of alkali components [13]. Zirconia refractories should also be designed to contain a higher percentage of fine pores for higher slag attack resistance, because slag attack intensifies as pore size increases in service [14].

Although the importance of castable AMZ microstructure in relation to the corrosion resistance was realised several decades ago, a detailed microstructural analysis has not been made so far. In the present work, an attempt has been made to understand the microstructural features of an AMZ refractory material penetrated by soda-lime-silica glass with the aid of scanning electron microscope.

2. Experimental procedure

Alumina–mullite–zircon (AMZ) composition was prepared by slip casting, where the phase composition of the refractory by weight% was given as follows: ~57% alumina, ~20% mullite, ~20% zircon, and ~3% clay. AMZ slip was taken and cast into a cubic piece of 75×75×75 mm^3, with a hole of 25 mm diameter and 25 mm depth in the middle of the piece. The piece was removed from the mould 24 h later. AMZ sample was dried in an oven at ~110 °C to remove any moisture from the piece, and fired at ~1600 °C for 2 h. Bulk density and apparent porosity were measured using the standard water immersion method [15]. Then, a standard soda-lime-silica glass, sieved through a 600 μm sieve, was put into the hole up to top of the AMZ sample. The sample was statically tested at 1370 °C for 72 h. It was then cut from the middle of the corroded area at the size of 20×20×5 mm^3. The polishing of specimen for optical and SEM examination was carried out using a Planopol/Pedemax automatic polishing machine. Using a CamScan 4 scanning electron microscope, back scattered electron images and relevant X-ray map distributions were then obtained to examine microstructural features at the interface region (between glass and refractory) of the corroded section. The semi-quantitative chemical analysis of five different areas located at an equal distance of approximately 500 μm from each other was performed using EDAX (Link ISIS 300) under the same microscope operating conditions.

3. Results and discussion

Bulk density and apparent porosity values of the AMZ sample are 2.9 g cm^{-3} and ~19%, respectively. The chemical compositions of glass and refractory used in this work are given in Table 1. A general microstructure of an AMZ material is illustrated in Fig. 1, showing the three regions, i.e. glass (g), interface (i) and refractory (r). At the interface region, the composition of each numbered zones (1–5) with a distance of ~500 μm length were analysed by EDAX. The results of those chemical analyses are given in Table 1.

As can be seen from Fig. 1, when the glass penetrated towards to the end of the interface zone, the number of the areas corroded by glass decreased markedly. When the glass started to penetrate into the pores at the edge of interface region (Zone I), randomly distributed small

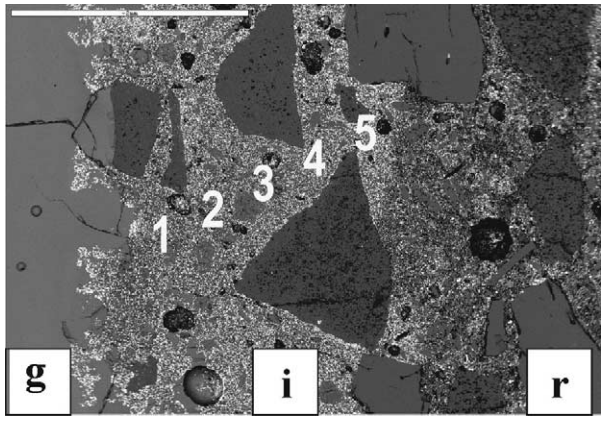

Fig. 1. Microstructure of an AMZ material, showing glass (g), interface (i), and refractory (r) regions (scale bar: 2 mm).

alumina particles located inside of the glassy phase were absorbed by the glass, where there were no zirconia particles around the pores (Fig. 2). During penetration, alumina particles started to dissolve in the glassy-phase region, and randomly oriented needle-like alumina crystals around 10–30 μm in length were formed due to the initiation of diffusion between the alumina particles and silica based glass. However, zirconia particles around the glassy-phase were dispersed homogeneously, and they prevented glass from penetrating into the pores in the zirconia-rich refractory phase, where the shape of the alumina particles did not change. Afterwards, the glassy zone in the interface region, which was ~500 μm away from the glass (Zone II), was examined. In Fig. 3, the needle-like alumina grains were seen to have grown in this glassy zone up to ~65 μm, because of higher solubility of alumina particles within the silica-calcium rich phase. The primary alumina grains in the refractory region were dissolved, and transported into the glassy phase. They were precipitated out much longer and randomly oriented needle-like alumina crystals, which is reminiscent of needle-like mullite formation in the silica-based glass. Fig. 4(a) shows that the length of the needle-like alumina crystals increased markedly up to 150 μm (Zone III). However, the alumina particles located within the zirconia-rich path remained their preliminary shape, and their growth rate was limited due to the presence of ZrO_2. The zirconia-rich phase made a very effective barrier amongst these glassy regions [Fig. 4(a)].

The rate of corrosion in an AMZ material at a high temperature, which is also affected by alkali components in the glasses, is governed by a process of zirconia-transport into bulk glasses and crystal decomposition. When the glass penetrated forward into the end of the interface region, the amount of Al_2O_3 and ZrO_2 increased whereas the contents of SiO_2, Na_2O and CaO decreased significantly (Table 1). Furthermore, CaO and K_2O contents were negligible between the end of the interface and the unreacted part of the refractory. The higher the diffusion of SiO_2, Na_2O and CaO from glass to refractory side, the higher the solubility of Al_2O_3 at the interface region (Table 1). As the alumina particles were entirely dissolved and transformed into the needle-like shape in a zircon-free glassy zone, alumina

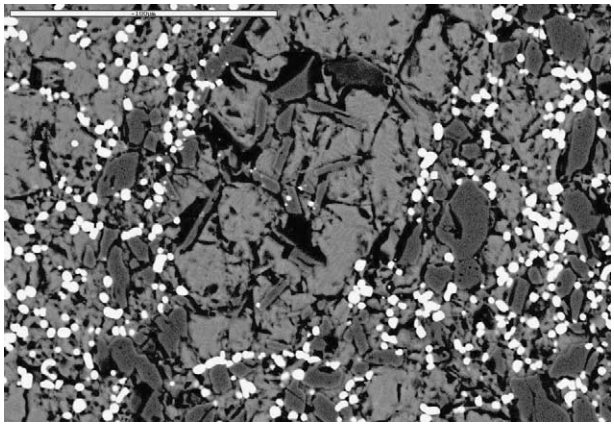

Fig. 2. Microstructure of AMZ, showing the initiation of glass penetration in Zone I (scale bar: 100 μm).

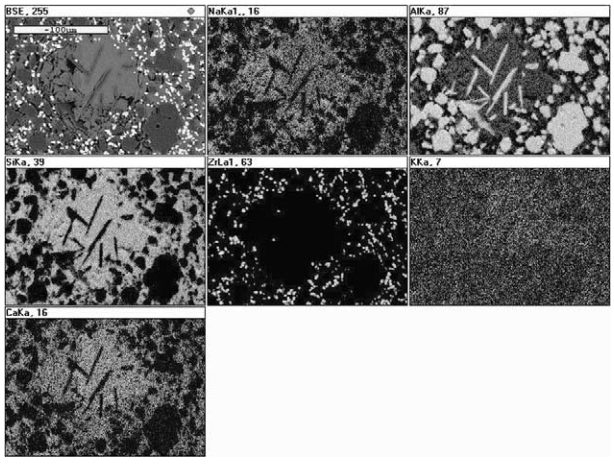

Fig. 3. Map distribution of AMZ in the interface region (Zone II: ~500 μm away from the glass).

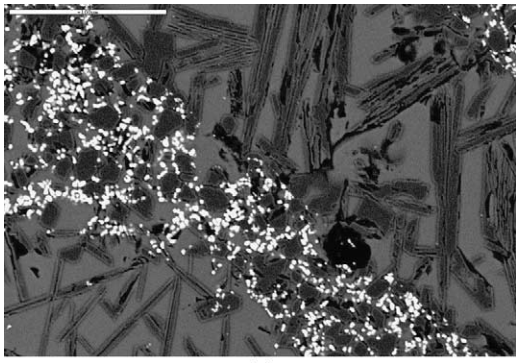

(a)

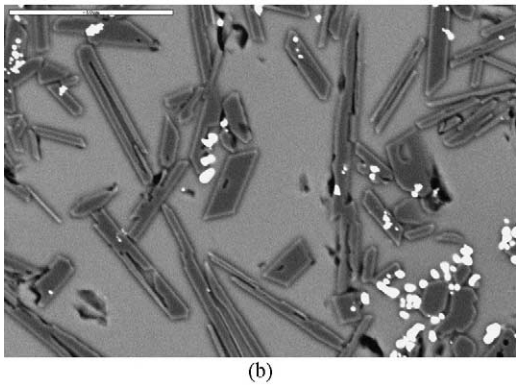

(b)

Fig. 4. Microstructure of AMZ in the interface region (Zone III: ~1000 μm away from the glass), showing: (a) a zirconia barrier between the glassy phases (scale bar: 100 μm); (b) randomly oriented needle-like alumina crystals (scale bar: 50 μm).

content also reached to a maximum level particularly in Zone III (Table 1), because of a high penetration rate, which led to a marked growth in the length of the needle-like particles. It was observed that there was a significant difference on the grain growth rate of needle-like particles, in comparison with the other penetrated zones. This morphology is also considered to be as a function of the different viscosities of the molten liquids present in each separate glassy phase zone. For this reason, the glass viscosity must be carefully controlled through its composition. A glassy phase formed in the penetrated region is viscous enough at elevated temperatures to deform and accommodate the large stresses

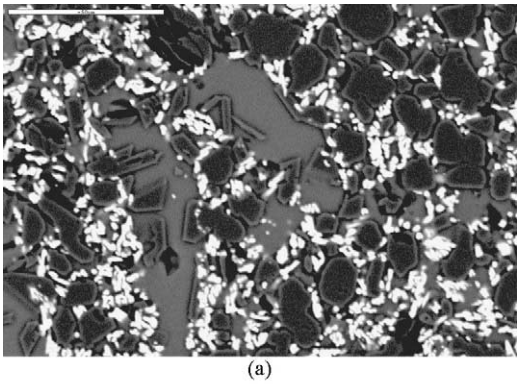

(a)

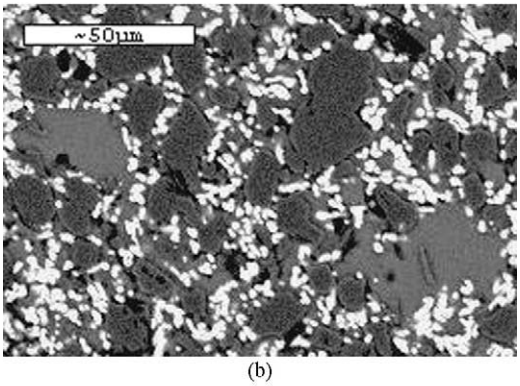

(b)

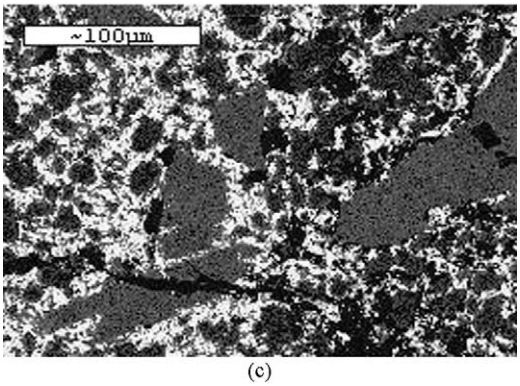

(c)

Fig. 5. Microstructure of AMZ, showing end of the interface region: (a) Zone IV: ~1000 μm away from the unreacted refractory (scale bar: 50 μm); (b) Zone V: ~500 μm away from the unreacted refractory; (c) at the end of the interface region and the unreacted refractory.

associated with the tetragonal to monoclinic ZrO_2 transition, which occurs at 1000–1200 °C on heating. The extension of needle-like alumina crystals in the glassy zone may cause an increased surface tension, with the gradient being equivalent to a shear stress leading forced convection, which may also explain the morphology of the glassy phase region.

Fig. 4(a) and (b) shows clearly that alumina grains were mechanically interlocked and difficult to be dislodged by ZrO_2 particles in the glassy zone. However, when the fine ZrO_2 particles were not embedded uniformly around the all alumina grains, the glassy phase was found to exhibit randomly oriented needle-like crystals, indicating that the major amount of alumina was found to be dissolved in the siliceous glassy phase. Fig. 5(a) illustrates that when the glass penetration approached to the unreacted refractory side, which was ~1 mm away from the refractory (Zone IV), the area of glassy phase decreased markedly. In addition, the formation of needle-like crystals, which were in the length of ~10 μm, was also limited, where some of them retained their original shape. Furthermore, when the glass reached to the end of the interface region (Zone V), the formation of needle-like alumina was negligible, with a significant reduction in the glassy phase area [Fig. 5(b)]. Fig. 5(c) showed that there were no randomly oriented needle-like crystals between the end of the interface region and the refractory. This is because ZrO_2 enhanced the corrosion resistance by interlocking the alumina particles, which were distributed and embedded in the fine ZrO_2 particles homogeneously. The corrosion resistance of AMZ arises from the unique microstructural features, including the interlocking of alumina crystals and the glassy phase with the most insoluble ZrO_2 crystals, indicating a low rate of dissolution of the Al_2O_3 at the end of the interface region.

4. Conclusions

Alumina had a much higher solubility than zirconia in the soda-lime-silica glass, and thus needle-like alumina crystals occurred during glass penetration. On the contrary, zirconia particles made an effective barrier in the corroded zone, and prevented glass from penetrating into the pores towards to the end of the penetration region, where no needle-like alumina crystals were observed. The corrosion resistance of AMZ arises from the unique microstructural features, which consist of interlocking of alumina crystals and the glassy phase with the most insoluble ZrO_2 crystals, resulting in a low rate of dissolution of Al_2O_3, SiO_2, Na_2O and CaO at the end of the interface region. ZrO_2 creates a more stable and durable interface, and raises the corrosion resistance of AMZ, leading to a long-life performance in service.

Acknowledgements

The author wishes to thank Professor F.L. Riley and Mr. F. Konieczny for their helpful discussions, and their invaluable expertise in this field was greatly appreciated.

References

[1] C. Aksel, The influence of zircon on the mechanical properties and thermal shock behaviour of slip-cast alumina-mullite refractories, Mater. Lett. 57(4) (2002) 992–997
[2] B.O. Mysen, Phase Diagrams for Ceramists, National Institute of Standards and Technology, The American Ceramic Soc. 8 (1990) 188.
[3] Y. Shi, X.X. Huang, D.S. Yen, Fabrication of hot-pressed zircon ceramics: mechanical properties and microstructure, Ceram. Int. 23 (5) (1997) 457–462.
[4] G. Orange, G. Fantozzi, F. Cambier, C. Leblud, M.R. Anseau, A. Leriche, High temperature mechanical properties of reaction-sintered mullite/zirconia and mullite/alumina/zirconia composites, J. Mater. Sci. 20 (1985) 2533–2540.
[5] S. Lathabai, D.G. Hay, F. Wagner, N. Claussen, Reaction-bonded mullite/zirconia composites, J. Am. Ceram. Soc. 79 (1) (1996) 248–256.
[6] I.M. Low, R.D. Skala, D.S. Perera, Fracture properties of layered mullite/zirconia-toughened alumina composites, J. Mater. Sci. Lett. 13 (18) (1994) 1334–1336.
[7] R.H.J. Hannink, Transformation toughening in zirconia-containing ceramics, J. Am. Ceram. Soc. 83 (3) (2000) 461–487.
[8] C. Aksel, F. Konieczny, Mechanical properties and thermal shock behaviour of PSR-333 alumina–mullite–zirconia refractory material, Glass International 24 (1) (2001) 16–18.
[9] L.J. Manfredo, R.N. McNally, The corrosion resistance of high ZrO_2-fusion-cast Al_2O_3–ZrO_2–SiO_2 glass refractories in soda lime glass, J. Mater. Sci. 19 (4) (1984) 1272–1276.
[10] D.E. Parkinson, Feeder and forehearth refractories, Glass Technology 29 (5) (1988) 173–176.
[11] T. Asokan, Microstructural features of fusion cast Al_2O_3–ZrO_2–SiO_2 refractories, J. Mater. Sci. Lett. 13 (1994) 343–345.
[12] A. Hawksworth, W.E. Lee, Microstructural observation of bottom drilling corrosion in electrocast Al_2O_3–ZrO_2–SiO_2 refractories, J. Mater. Sci. Lett. 15 (1996) 1702–1704.
[13] K. Kato, N. Araki, The corrosion of zircon and zirconia refractories by molten glasses, J. Non-Cryst. Solids 80 (1–3) (1986) 681–687.
[14] K.J. Chen, Y.C. Ko, Evaluation of zirconia refractories for continuous-casting, Am. Ceram. Soc. Bull. 62 (9) (1983) 1030–1035.
[15] British Standard Testing of Engineering Ceramics, BS 7134 Section 1.2, 1989.